RSC Advances

PAPER

View Article Online
View Journal | View Issue

Cite this: *RSC Adv.*, 2020, **10**, 18594

Assembly of lignin-based colloidal particles: effects of cationic surfactants, molecular weight, and solvent on morphology†

Dexiang Liu,[a] Jinyu Liu,[a] Yingxiang Zhou,[a] Jienan Chen,[abcd] Peng Zhan,[abcd] Guoen Yang[a] and Zhiping Wu *[abcd]

Sodium lignosulfonate (LS) is a lignin derivative, which has abundant resources and is an environmentally friendly raw material. In this study, cetyltrimethylammonium bromide (CTAB) and stearyltrimethylammonium bromide (STAB) were combined with LS at the isoelectric point for hydrophobic self-assembly. Transmission electron microscopy (TEM), Fourier-transform infrared (FTIR) spectroscopy, and static contact angle data proved that LS/CTAB could form colloidal spheres, while LS/STAB could not form such spheres. The impact of the molecular weight of LS on the self-assembly of LS/CTAB was investigated by using the TEM, FTIR, and static contact angle data. The obtained results showed that LS/CTAB with 10 000–50 000 Da of LS could form colloidal spheres, while LS/CTAB with 3000–5000 Da of LS could not. In addition, the TEM images revealed that the solvent plays an important role in the morphology of LS/CTAB colloidal spheres. Finally, LS/CTAB colloidal spheres were used for the encapsulation of ibuprofen (IBU). The *in vitro* release behavior of IBU was proven to be pH-sensitive and exhibited controlled release properties. More than 85% IBU could be preserved in simulated gastric fluid, and over 75% could be released in simulated intestinal fluid. This work provides a theoretical basis for the preparation of LS/CTAB colloidal spheres and facilitates the expansion of its applications as a drug carrier.

Received 14th February 2020
Accepted 29th April 2020

DOI: 10.1039/d0ra01444c

rsc.li/rsc-advances

1 Introduction

As one of the most popular new materials, micro-/nanoparticles have unique photoelectric and chemical properties, adjustable mechanical properties, and larger specific surface area than those obtainable from traditional materials. They have been applied in many fields such as energy storage,[1] electronic devices,[2] micromotors,[3] catalysts and catalytic carriers,[4] medicine,[5] industry, and agriculture.[6] However, with an increase in resource consumption, along with increased environmental pollution and toxicity of the prepared materials (particularly in biomedicine), the requirements for materials have become more stringent. This has prompted researchers to develop newer technologies and search for green raw materials to resolve such dilemmas.[5,7]

Lignin is the second most ample environmentally friendly biomass raw material available in nature (after cellulose), which can be used in the preparation of synthetic polymer materials, and it is expected to replace fossil resources.[8–10] Lignin contains functional groups such as phenolic hydroxyl, aliphatic hydroxyl, carbonyl group, and carboxyl group, which can be formulated into various micro-/nanoparticles.[11–13] Self-assembly is a worthwhile strategy to form micro-/nanoparticles owing to their amphiphilic properties.[14–18] Lignosulfonate is a typical derivative of lignin, which is obtained *via* the sulfite pulping process.[19,20] However, sodium lignosulfonate (LS) exhibits very severe hydrophilicity owing to the presence of strongly hydrophilic sulfonic groups on the LS molecule; consequently, the hydrophobic self-assembly of LS is extremely difficult. Hydrophobic modification is required to perform the hydrophobic self-assembly of LS;[21] nevertheless, the chemical modification of LS may generate toxicity toward the body and can consume a large amount of chemicals, which are adverse to the applications of LS as drug carrier materials.[22]

Therefore, a new nontoxic physical modification method has been designed; according to this method, LS containing many charge groups was combined with the green cationic surfactant, CTAB (which exhibited good biodegradability and bactericidal properties), *via* electrostatic interactions to enhance the hydrophobicity of LS. Accordingly, LS/CTAB colloidal spheres were prepared by self-assembly without necessitating any

[a]School of Materials Science and Engineering, Central South University of Forestry and Technology, Changsha, 410004, China. E-mail: wuzhiping02@163.com
[b]Ministry of Forestry Bioethanol Research Center, Central South University of Forestry and Technology, Changsha, 410004, China
[c]Hunan Engineering Research Center for Woody Biomass Conversion, Central South University of Forestry and Technology, Changsha, 410004, China
[d]Hunan International Joint Laboratory of Woody Biomass Conversion, Central South University of Forestry and Technology, Changsha, 410004, China

† Electronic supplementary information (ESI) available. See DOI: 10.1039/d0ra01444c

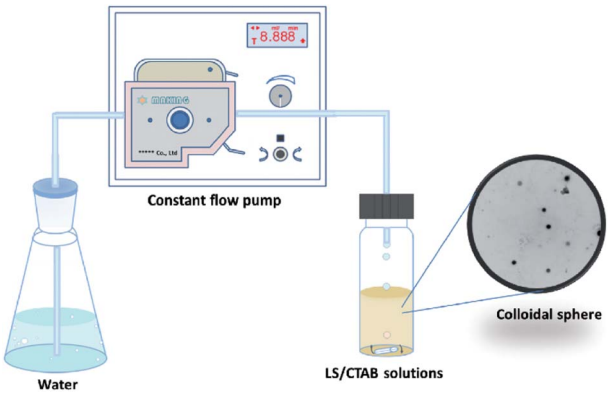

Fig. 1 Schematic of the preparation process.

chemical modification.[23] For example, Li *et al.* achieved the free conversion of the aggregation and disaggregation of LS/CTAB particles by adjusting the hydrophilic and hydrophobic surroundings of the system; further, LS/CTAB particles were used to wrap the photosensitive pesticide Avermectin (AVM) to improve the anti-photodegradation properties of AVM@LS/CTAB.[24] In addition, Qiao *et al.* reported that LS was first modified by CTAB to increase its hydrophobicity; then, they transformed LS/CTAB colloidal particles from spherical to vesicular morphology by adjusting the dose of tetraethyl orthosilicate, which was applied toward the encapsulation of doxorubicin.[25] However, the influence of the types of cationic surfactants on LS self-assembly has not been extensively investigated. Furthermore, LS has a wide range of molecular weight distributions; the impact of molecular weight on LS self-assembly has not been reported, which adversely impacts the applications of LS colloidal spheres as a carrier. Further studies regarding the effects of the cationic surfactant, molecular weight, and solvents on the assembly process are still necessary and meaningful.

In this paper, the preparation process of colloidal particles is shown in Fig. 1. The mixture solution is dissolved in an ethanol solution, following which water is added to the ethanol system *via* a peristaltic pump. The LS/CTAB mixture was successfully assembled into colloidal spheres. The influence of cationic surfactants and LS molecular weight on the formation of colloidal spheres was investigated by using transmission electron microscopy (TEM), static contact angle, and Fourier-transform infrared (FTIR) spectroscopy measurements. Then, the effect of the solvent on the morphology was investigated by TEM. Finally, the encapsulation of drugs and *in vitro* release performance with composite particles were also investigated. This research can facilitate the expansion of its applications as drug carriers.

2 Experimental section

2.1 Materials

Commercial LS was provided by Fucheng Chemical Reagent Co. (Tianjin, China). Raw LS was processed by filtration. LS samples with 3000–5000, 5000–10 000, and 10 000–50 000 Da were obtained by an ultrafiltration instrument equipped with ultrafiltration membranes of 3000, 5000, 10 000, and 50 000 Da, which were purchased from Haoqing Environmental Protection Technology Co. (Shanghai, China). Cetyltrimethylammonium bromide (CTAB) and stearyltrimethylammonium bromide (STAB) were of the analytical grade and purchased from Mackin Chemical Reagent Co., Ltd. (Shanghai, China). Ibuprofen (IBU) was purchased from Mackin Chemical Reagent Co., Ltd. (Shanghai, China). Others chemical reagents of the analytical grade were purchased from Sinopharm Chemical Reagent Co., Ltd. (Tianjin, China) and were used without further treatment.

2.2 Preparation of lignin-based colloidal particles

First, 50 wt% LS aqueous solution (2 g LS and 2 g deionized water) and 50 wt% cationic surfactant of EtOH/H_2O (m/m, 3/2) solution (2 g CTAB or STAB, 1.2 g EtOH, and 0.8 g deionized water) were prepared. Subsequently, these two solutions were mixed in a certain proportion, stirred for 30 min, and set aside for 2 h to afford LS/CTAB or LS/STAB mixtures. Second, a mixture with 2.0 mg LS/CTAB solids was dissolved by adding 2.0 mL EtOH under stirring at 550 rpm to prepare solid content of 1 mg mL^{-1}. Finally, water was added dropwise into the mixture solution at the rate of 0.50 mL min^{-1} by a peristaltic pump until the water content reached 90 vol%; further, the reaction was continually stirred for 2 h to stabilize the colloidal system.

2.3 Determination of the loading ability and encapsulation efficiency of LS/CTAB@IBU

IBU-loaded micelles were prepared following a process similar to the preparation of LS/CTAB colloidal particles. Briefly, 60 mg IBU and 40 mg LS/CTAB (a complex of LS/CTAB was prepared at the isoelectric point, *i.e.*, m(CTAB) : m(LS) = 0.7307, and then the complex was freeze-dried) were dissolved in 20 mL EtOH by stirring for 20 min. Then, water was added dropwise into this mixture solution at the rate of 2.0 mL min^{-1} by a peristaltic pump until the water content reached 90 vol%. The reaction was continually stirred for 2 h and the solution underwent micellization as the water content increased, forming IBU-loaded colloidal particles (LS/CTAB@IBU). EtOH was recovered by rotary evaporation, and LS/CTAB@IBU was collected by centrifugation. Raw LS/CTAB@IBU was washed 3 times to remove the residual IBU and LS/CTAB and then LS/CTAB@IBU was freeze-dried for 24 h as the reserve.

First, 10 mg LS/CTAB@IBU was mixed with 25 mL methanol and placed in an ultrasonic bath for 30 min. The resulting IBU extracts were collected by filtering with an organic membrane (0.45 μm), and the IBU content in methanol was determined by high-performance liquid chromatography (HPLC). The IBU loading and encapsulation efficiency were calculated according to eqn (1) and (2), respectively:

$$\text{IBU loading}(\%) = \left(\frac{\text{weight of IBU loaded}}{\text{weight of LS/CTAB@IBU}}\right) \times 100 \quad (1)$$

$$\text{Encapsulation efficiency}(\%) = \left(\frac{\text{weight of IBU loaded in LS/CTAB@IBU}}{\text{initial amount of IBU}}\right) \times 100 \quad (2)$$

2.4 Controlled release of IBU and *in vitro* drug release studies

Briefly, 10 mg LS/CTAB@IBU was suspended in 10 mL simulated gastric fluid (SGF, 0.064 M HCl, 0.05 M KCl, pH 1.2) or simulated intestinal fluid (SIF, 8.0000 g NaCl, 0.2001 g KCl, 1 L phosphate buffer, pH 7.3) and transferred into a dialysis bag (MWCO: 3500 Da). The dialysis bag was immersed in 40 mL SGF or SIF and then placed in a shaking incubator at a constant temperature of 37 °C. Then, 1 mL of the sample was periodically collected, and the same volume of fresh buffer was added to maintain the total volume. Simultaneously, the IBU concentrations in the different samples were determined by HPLC.

For the *in vitro* drug release studies, a dialysis bag containing 10 mL SGF and 10 mg LS/CTAB@IBU was immersed in 40 mL SGF and then incubated at 37 °C. Here, 1 mL of the sample was periodically collected, and the same volume of fresh buffer was added to maintain the total volume. After incubation for 2 h, the dialysis bag was centrifuged in a centrifuge tube and SGF in the dialysis bag was collected as much as possible. Then, the dialysis bag was placed in 50 mL SIF to continue incubation. At the same time, 1 mL of the sample was collected at different time intervals, and 1 mL of fresh SIF was added to maintain the total volume. The sample containing IBU was determined by HPLC.

2.5 Characterizations

A Zetasizer Nano ZS90 instrument was used to analyze the particle size (average hydrodynamic diameter), polydispersity index (PDI), and zeta potential of the samples. The sample was put into a cuvette and maintained under equilibrium at 25 °C for 2 min prior to performing the measurements. The data was collected by using a Zetasizer Nano ZS90 (Malvern Instruments, Malvern, UK) instrument. The data from the three replicates were averaged.

TEM images were acquired using a Hitachi H-7650 electron microscope (Hitachi, Japan) at an accelerating voltage of 80 kV. The TEM samples were prepared by dropping diluted dispersions onto copper grids coated with a thin carbon film and then drying for 24 h at room temperature.

The contact angle of water on the mixture disks were determined using an OCA 15 static contact angle measurement instrument (DataPhysics Instruments GmbH, Germany). The dried sample powder was pressed into disks (1 cm^2) at 10 MPa for 2 min for performing the measurement. A 4 μL water droplet was dropped onto this mixture disk; after 5 s, the images of the sample/water interface were taken through a microscope in the instrument. The contact angle was calculated *via* hypsometry. Three replicates were obtained for each sample.

The FTIR spectra of the samples were recorded using a FTIR spectrometer (Bruker Alpha, Bruker, Germany) using a potassium bromide disc containing 1 wt% of finely ground samples. Thirty-two scans were taken for each sample in the range of 4000–500 cm^{-1} at a resolution of 2 cm^{-1} in the transmittance mode.

The IBU content in solution was determined by means of HPLC (Agilent ZORBAX, Agilent, USA) with the isocratic elution of a methanol–phosphate-buffered solution (75/25, v/v; pH 5.0) as the mobile phase. Then, 20 μL of the sample was injected into the HPLC system and separated at 40 °C using a flow rate of 1 mL min^{-1} with a detection wavelength of 222 nm. Three replicates were obtained for each sample.

3 Results and discussions

3.1 Effects of cationic surfactants

Cationic surfactants have an important influence on the self-assembly of LS; there are several kinds of cationic surfactants. Here, we selected CTAB and STAB with certain hydrophobicity as the cationic surfactants (Fig. S1;† at the isoelectric point, m(CTAB) : m(LS) = 0.7307 and m(STAB) : m(LS) = 0.5888). The cations and anions of LS were combined by electrostatic attraction (Fig. 7), which improve the overall hydrophobicity of LS. The influences of CTAB and STAB on the assembly of colloidal particles were explored. Fig. 2a and b show the TEM images of the self-assembled products of LS/CTAB and LS/STAB. The spherical morphology (as shown in Fig. 2a) clearly demonstrates that the diameter of the colloidal spheres is about 470 nm. However, irregular aggregates can be observed (Fig. 2b), which can be attributed to the presence of pure LS.[26] Meanwhile, some tiny particles (10–25 nm) were also observed (inset of Fig. 2b), which may be LS or STAB particles. This indicates that only the LS/CTAB complex was successfully assembled into a colloidal sphere, while the LS/STAB complex failed to form a colloidal sphere.

In order to further explore the interaction between LS with CTAB and STAB, static contact angles were measured for the

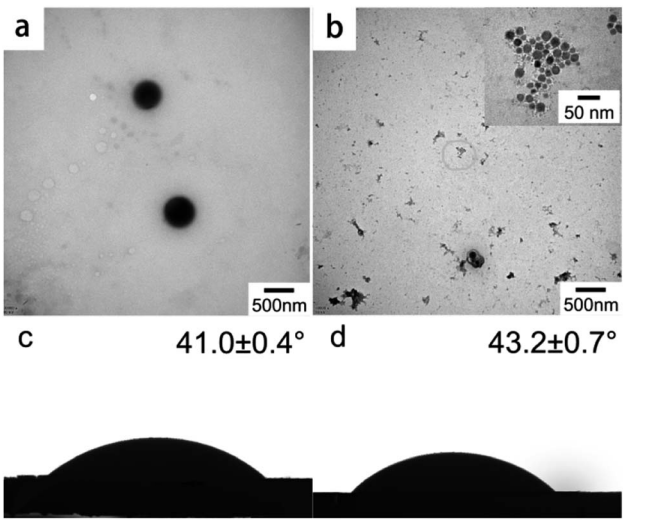

Fig. 2 TEM images and static contact angles of LS/CTAB (a and c) and LS/STAB (b and d).

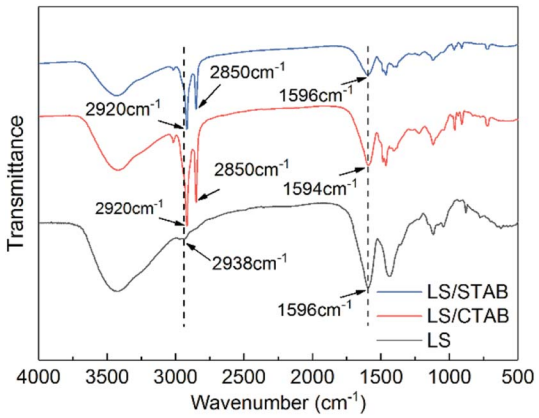

Fig. 3 FTIR spectral analysis of LS, LS/CTAB, and LS/STAB.

water droplets on the LS/CTAB and LS/STAB samples. The obtained results are shown in Fig. 2c and d. The static contact angles of water on LS/CTAB and LS/STAB disks were 41.0 ± 0.4° and 43.2 ± 0.7°, respectively, indicating that the hydrophobicity of LS/STAB is higher than that of LS/CTAB. However, it is difficult for LS to form a colloidal sphere with the more hydrophobic STAB, which can be explained from the details of the self-assembly process. Although the hydrophobicity of LS/STAB is higher than that of LS/CTAB, LS/STAB can decompose during self-assembly owing to the extremely poor water solubility of STAB, resulting in the weak binding ability of LS/STAB and the failure of colloidal formation. The inset in Fig. 2b further proves this conclusion; the tiny particles observed in the insets are STAB particles.

Moreover, the occurrence of self-assembly requires certain interactions, namely, van der Waals forces, electrostatic interactions, hydrogen bonds, capillary phenomena, π–π interactions, *etc.*[27–29] Moreover, π–π interactions play a crucial role in the self-assembly of lignin.[30] Therefore, we determined the infrared spectrum of the samples to understand the π–π interactions; the obtained results are shown in Fig. 3. In the FTIR spectra of LS/CTAB and LS/STAB, sharp C–H stretching vibration peaks of alkanes (2920 and 2850 cm^{-1}) are evident, while the C–H stretching vibration peaks in LS alkanes are at 2938 cm^{-1} with a weak peak, indicating the presence of CTAB and STAB in the complex, respectively. By comparing the C–H characteristic peaks of the aromatic skeletons of LS, LS/CTAB, and LS/STAB, it is evident that all the characteristic peaks of the aromatic skeletal vibrations of LS and LS/STAB are at 1596 cm^{-1}, while the characteristic peak of the aromatic skeleton of LS/CTAB is at 1594 cm^{-1}; these data indicate an environmental change in the benzene ring of LS in LS/CTAB. This result is consistent with the data reported in the literature regarding changes in the benzene ring environment due to π–π aggregation.[23] This FTIR analysis further proves the decomposition of LS/STAB during the assembly process. Moreover, this provides a theoretical basis for the selection of cationic surfactants to form LS colloidal spheres.

3.2 Effect of the molecular weight of LS

The molecular weight affects the properties of the material and has a certain effect on the self-assembly process.[31] The molecular weight distribution of LS is very wide, ranging from thousand to several tens of thousands of units, which is determined by the source of the raw materials as well as the treatment methods.[32,33] In order to investigate the effect of molecular weight of LS on the self-assembly of colloidal particles, CTAB was used to hydrophobically modify LS of different molecular weights and then self-assemble into LS/CTAB colloidal particles (zeta potential of CTAB and LS with different molecular weights at the isoelectric point are shown in Fig. S2†). Fig. 4 shows the TEM images of the self-assembled product. There are large "floating cloud" aggregates without any spherical morphology, as shown in Fig. 4a. However, microspheres are fairly evident, as shown in Fig. 4c. Interestingly, there are many tiny particles (~50 nm), as shown in Fig. 4b. This indicates that only LS/CTAB (LS: 10 000–50 000 Da) can be self-assembled into microspheres.

In order to reveal the reason for this phenomenon, the static contact angles of the samples were measured, and the obtained results are shown in Fig. S3.† The contact angles of deionized water on LS/CTAB-*b* and LS/CTAB-*c* disks are 39.8 ± 0.9° and 52.0 ± 0.2°, respectively. Obviously, these contact angles are

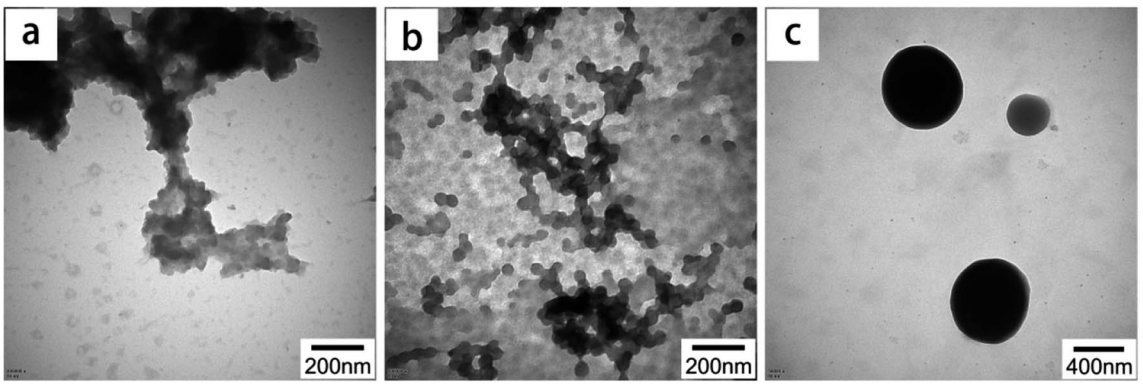

Fig. 4 TEM images of LS/CTAB with different molecular weights of LS ((a) 3000–5000 Da of LS (LS/CTAB-*a*); (b) 5000–10 000 Da of LS (LS/CTAB-*b*); (c) 10 000–50 000 Da of LS (LS/CTAB-*c*)).

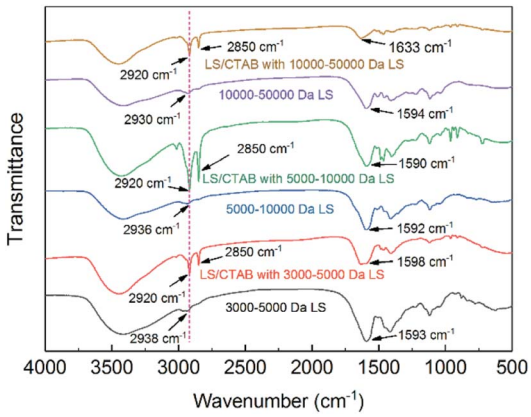

Fig. 5 FTIR spectral analysis of LS and LS/CTAB complexes with different molecular weights.

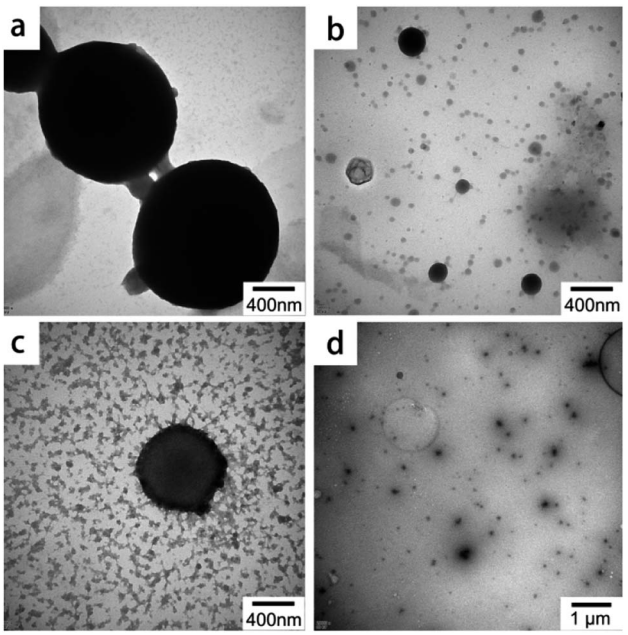

Fig. 6 TEM images of LS/CTAB with different good solvents ((a) EtOH; (b) DMSO; (c) THF; (d) 1,4-dioxane).

similar to those of LS/CTAB (Fig. 2c); consequently, CTAB can be shown to improve the hydrophobicities of both LS/CTAB-*b* and LS/CTAB-*c*. However, the contact angle of water on LS/CTAB-*a* cannot be detected due to its strong hydrophilicity. This indicates that the hydrophobicity of low-molecular-weight LS cannot be increased by CTAB, resulting in the failure of hydrophobic self-assembly. Higher-molecular-weight LS has a lower zeta potential than lower-molecular-weight LS (Fig. S2†), indicating that the electrostatic effect of higher-molecular-weight LS is higher than that of lower-molecular-weight LS. Therefore, higher-molecular-weight LS and CTAB exhibit stronger electrostatic attraction, thereby tuning the hydrophobicity of higher-molecular-weight LS. However, lower-molecular weight LS and CTAB may only play the role of neutralizing the charge at the isoelectric point.

For further understanding environmental changes in the benzene ring of LS, the infrared spectra of the samples were determined. As shown in Fig. 5, when comparing the C–H stretching vibration peaks of the aromatic skeletons of all the samples, it was found that the aromatic skeletal characteristic peaks of all the complexes were shifted. Nevertheless, molecular aggregation did not always result in π–π aggregation, and the reverse is also true;[34] however, combining the data shown in Fig. 4 and 5, we can conclude that π–π aggregation must exist in the LS/CTAB complex system with 5000–10 000 Da of LS and 10 000–50 000 Da of LS. According to the formation mechanism of LS/CTAB colloidal spheres, colloidal spheres are formed by the aggregation of individual clusters.[23] Further, small molecular surfactants can promote the disaggregation of lignin.[35] Therefore, we speculate that LS/CTAB with 5000–10 000 Da of LS only formed 50 nm particles owing to the fact that lower-molecular-weight LS and CTAB promote the disaggregation of LS/CTAB microspheres.

3.3 Effect of solvents

Hydrophobic self-assembly involves a process initiated by a good solvent/antisolvent, which shows that the solvent has an important effect on self-assembly (such as morphology).[31,36,37] In this work, ethanol was used as the good solvent and water, the antisolvent. Moreover, dimethyl sulfoxide (DMSO), tetrahydrofuran (THF), and 1,4-dioxane were also studied as other good

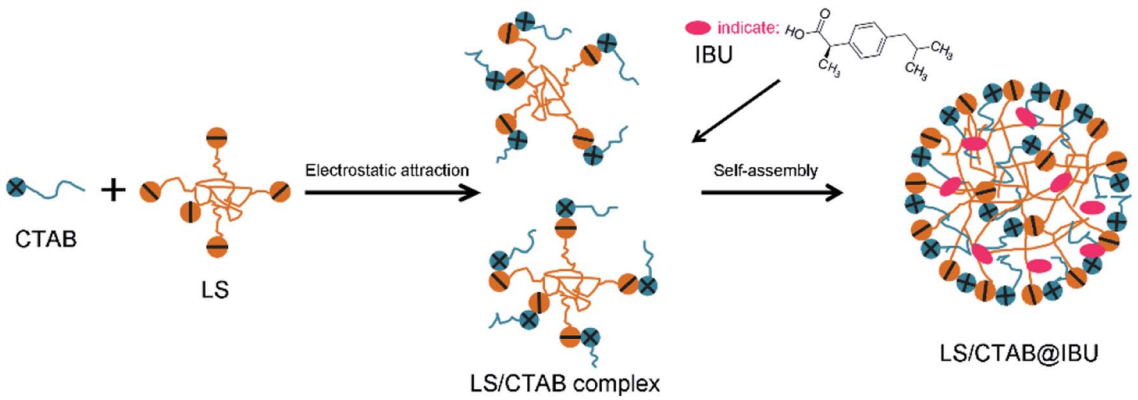

Fig. 7 Proposed schematic for the formation of LS/CTAB@IBU.

Table 1 IBU loading rate, encapsulation efficiency, and solid sample yield values of LS/CTAB@IBU samples

Sample[a]	Theoretical IBU loading[b]	IBU loading	Solid sample yield[c]	Encapsulation efficiency
LS/CTAB@IBU-1	33.33%	32.99 ± 0.02%	50.82 ± 0.27%	50.30 ± 0.33%
LS/CTAB@IBU-2	50%	53.62 ± 0.07%	55.43 ± 0.09%	59.44 ± 0.03%
LS/CTAB@IBU-3	66.67%	63.27 ± 0.13%	70.71 ± 0.98%	67.11 ± 1.12%

[a] The mass ratios of LS/CTAB/IBU in LS/CTAB@IBU-1, LS/CTAB@IBU-2, and LS/CTAB@IBU-3 are 1/0.5, 1/1, and 1/2, respectively. [b] Theoretical IBU loading (%) = (weight of IBU used to prepare the LS/CTAB@IBU/total weight of the solid components used in the experiment) × 100%. [c] Solid sample yield = (total weight of the recovered sample/total weight of the solid components used in the experiment) × 100%.

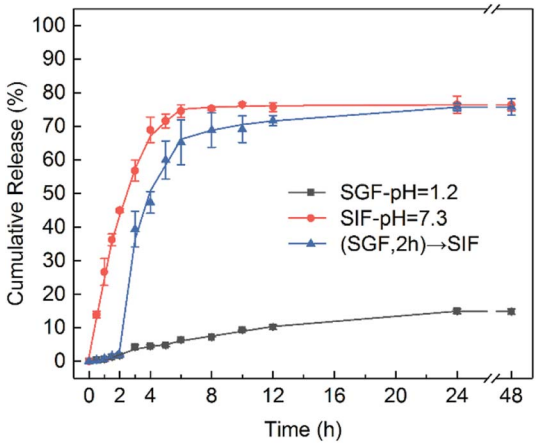

Fig. 8 *In vitro* release profiles of IBU-encapsulated LS/CTAB colloidal spheres in SGF (pH 1.2) and SIF (pH 7.3).

solvents; the corresponding TEM images are shown in Fig. 6. Microspheres with an uneven size can be clearly observed, as shown in Fig. 6b, while many "floating cloud" clusters are visible in Fig. 6c; local clusters can be observed in Fig. 6d. The morphology of the microspheres shown in Fig. 6a reveals that ethanol is the best choice among these good solvents, which may be attributed to the solubility order of CTAB in these organic solvents.

3.4 Controlled release behaviors and *in vitro* release studies

Lignin-based materials have been widely used as a drug carrier owing to their natural character, low cost, and safety toward normal human cells.[22,38] However, the potential of LS/CTAB colloidal particles as an oral drug carrier has not been assessed. In this work, IBU was selected as the oral model of a hydrophobic drug that could dissolve in an ethanol solution contain the LS/CTAB complex; subsequent to the addition of water to the ethanol system, IBU was successfully encapsulated into LS/CTAB colloidal spheres (Fig. 7). The IBU loading rate and encapsulation efficiency values of LS/CTAB are shown in Table 1. Evidently, the encapsulation efficiencies of LS/CTAB colloidal spheres increased from 50.30% to 67.11% with an increase in IBU content. This shows that LS/CTAB colloidal spheres exhibit good encapsulation over IBU.

To assess the *in vitro* release performance of LS/CTAB@IBU, LS/CTAB@IBU-3 was incubated in SGF (pH 1.2) and SIF (pH 7.3) at 37 °C for 48 h. The release kinetics are shown in Fig. 8. At pH 1.2, the drug release rate was slow, with only 6.35% of IBU released after 6 h and 14.81% after 48 h; moreover, the release reached saturation within 24 h. At pH 7.3, about 74.55% IBU was released after 6 h, almost reaching saturated release (48 h, 76.46%). This indicates that the drug can be effectively protected from the severe environment of the stomach and can exhibit rapid release under simulated intestinal conditions. Considering the fact that an oral drug passes from the stomach to the intestine in the human body, LS/CTAB@IBU-3 was firstly incubated in SGF for 2 h and then transferred to SIF for further incubation.[39–41] As shown in Fig. 8, only 1.77% IBU was released after 2 h, while the release of IBU accelerated when LS/CTAB@IBU-3 was transferred to SIF; subsequently, 75.76% IBU was released after 24 h, reaching release saturation. The result of this "biomimetic" evaluation reveals that the drug release profile of LS/CTAB@IBU is pH-sensitive. This phenomenon may be attributed to several synergistic factors. The first factor is the ionization of the carboxyl groups in LS, which contributes toward the dissociation of the colloidal structure; consequently, the entrapped IBU is completely released in the intestinal tract.[41] The second factor is electrostatic repulsion between the negatively charged carboxyl groups of IBU and negatively charged LS (carboxyl groups, hydroxyl groups, and sulfonate groups). The last factor is the higher solubility of IBU at pH 7.3.[42] These factors indicate that LS/CTAB colloidal spheres enabled drug release to preferentially occur in the intestine while preventing drug leakage in the stomach. These release profiles meet the requirements of oral administration. This implies that LS/CTAB colloidal particles possess potential applications as an oral drug carrier.

4 Conclusions

Lignin-based colloidal spheres have attracted considerable attention due to their worthwhile antioxidation characteristics, UV resistance, degradation, and abundant resources. In this paper, CTAB and STAB were combined with LS *via* electrostatic attractions to improve the hydrophobicity of LS; only LS/CTAB was successfully assembled into colloidal spheres, while LS/STAB complexes decomposed during the self-assembly process and failed to form microspheres owing to the poor water solubility of STAB. Moreover, the molecular weight of LS has a drastic influence on the self-assembly process. The larger molecular weight results in the higher hydrophobicity of the LS/CTAB complex as well as the ease toward forming colloidal spheres. In addition, the TEM images revealed that ethanol is

a good solvent toward LS/CTAB. The drug encapsulation efficiency and release rate during *in vitro* studies with IBU-encapsulated LS/CTAB colloidal spheres confirmed pH dependence. Less than 15% of the loaded IBU was released in SGF over 48 h, but about 75% of the oral drug was released within 6 h in SIF. This shows the potential of this LS system as an oral drug carrier. In summary, this work provides a theoretical basis for the preparation of LS/CTAB colloidal spheres and to facilitate its improved applicability as a drug carrier.

Conflicts of interest

There are no conflicts to declare.

Acknowledgements

We gratefully acknowledge the financial supports from the National Key R&D Program of China (2017YFD0601004), Open Fund of Forestry Engineering, Central South University of Forestry and Technology.

Notes and references

1 J. Nai and X. W. Lou, *Adv. Mater.*, 2019, **31**, 1706825.
2 B. Yin, X. Liu, H. Gao, T. Fu and J. Yao, *Nat. Commun.*, 2018, **9**, 5161.
3 Y. Ji, X. Lin, H. Zhang, Y. Wu, J. Li and Q. He, *Angew. Chem., Int. Ed.*, 2019, **58**, 4184–4188.
4 B. Li and H. C. Zeng, *Adv. Mater.*, 2019, **31**, 1801104.
5 I. Khan, K. Saeed and I. Khan, *Arabian J. Chem.*, 2019, **12**, 908–931.
6 C. Peng, Z. Chen and M. K. Tiwari, *Nat. Mater.*, 2018, **17**, 355–360.
7 W. H. De Jong and P. J. A. Borm, *Int. J. Nanomed.*, 2008, **3**, 133–149.
8 D. Kai, M. J. Tan, P. L. Chee, Y. K. Chua, Y. L. Yap and X. J. Loh, *Green Chem.*, 2016, **18**, 1175–1200.
9 D. M. Rocca, J. P. Vanegas, K. Fournier, M. C. Becerra, J. C. Scaiano and A. E. Lanterna, *RSC Adv.*, 2018, **8**, 40454–40463.
10 R. Vanholme, B. Demedts, K. Morreel, J. Ralph and W. Boerjan, *Plant Physiol.*, 2010, **153**, 895.
11 P. Figueiredo, K. Lintinen, J. T. Hirvonen, M. A. Kostiainen and H. A. Santos, *Prog. Mater. Sci.*, 2018, **93**, 233–269.
12 W. Zhao, B. Simmons, S. Singh, A. Ragauskas and G. Cheng, *Green Chem.*, 2016, **18**, 5693–5700.
13 D. Yiamsawas, G. Baier, E. Thines, K. Landfester and F. R. Wurm, *RSC Adv.*, 2014, **4**, 11661–11663.
14 Y. Qian, Y. Deng, X. Qiu, H. Li and D. Yang, *Green Chem.*, 2014, **16**, 2156–2163.
15 H. Li, Y. Deng, B. Liu, Y. Ren, J. Liang, Y. Qian, X. Qiu, C. Li and D. Zheng, *ACS Sustainable Chem. Eng.*, 2016, **4**, 1946–1953.
16 F. Xiong, Y. Han, S. Wang, G. Li, T. Qin, Y. Chen and F. Chu, *Ind. Crops Prod.*, 2017, **100**, 146–152.
17 J. Wang, B. Wu, S. Li, G. Sinawang, X. Wang and Y. He, *ACS Sustainable Chem. Eng.*, 2016, **4**, 4036–4042.
18 X. Rao, Y. Liu, Q. Zhang, W. Chen, Y. Liu and H. Yu, *ACS Omega*, 2017, **2**, 2858–2865.
19 Y. Qian, H. Lou, W. Liu, D. Yang, X. Ouyang, Y. Li and Q. Xueqing, *Tappi J.*, 2018, **17**, 125–141.
20 K. M. Askvik, S. Hetlesæther, J. Sjöblom and P. Stenius, *Colloids Surf., A*, 2001, **182**, 175–189.
21 N. Hong, Y. Li, W. Zeng, M. Zhang, X. Peng and X. Qiu, *RSC Adv.*, 2015, **5**, 21588–21595.
22 M. H. Sipponen, H. Lange, C. Crestini, A. Henn and M. Österberg, *ChemSusChem*, 2019, **12**, 2039–2054.
23 Q. Tang, M. Zhou, Y. Li, X. Qiu and D. Yang, *ACS Sustain. Chem. Eng.*, 2018, **6**, 1379–1386.
24 Y. Li, M. Zhou, Y. Pang and X. Qiu, *ACS Sustainable Chem. Eng.*, 2017, **5**, 3321–3328.
25 X. G. Qiao, H. J. Wu, Z. Zhou, Q. Q. Tang, X. C. Pang, M. X. Zang and S. Z. Zhou, *Ind. Crops Prod.*, 2019, **135**, 64–71.
26 X. Qiu, Q. Kong, M. Zhou and D. Yang, *J. Phys. Chem. B*, 2010, **114**, 15857–15861.
27 G. M. Whitesides and B. Grzybowski, *Science*, 2002, **295**, 2418.
28 J.-M. Lehn, *Science*, 2002, **295**, 2400.
29 B. M. Rosen, C. J. Wilson, D. A. Wilson, M. Peterca, M. R. Imam and V. Percec, *Chem. Rev.*, 2009, **109**, 6275–6540.
30 Y. Deng, X. Feng, M. Zhou, Y. Qian, H. Yu and X. Qiu, *Biomacromolecules*, 2011, **12**, 1116–1125.
31 B. Zhao, R. T. Haasch and S. MacLaren, *J. Am. Chem. Soc.*, 2004, **126**, 6124–6134.
32 S. M. Braaten, B. E. Christensen and G. E. Fredheim, *J. Wood Chem. Technol.*, 2003, **23**, 197–215.
33 M. F. Yan, X. Q. Qiu, D. J. Yang and H. U. Wen-Li, *Chem. J. Chin. Univ.*, 2008, **29**, 2312–2316.
34 Y. Deng, Y. Li and X. Wang, *Macromolecules*, 2006, **39**, 6590–6598.
35 Y. Li, D. Yang, S. Lu, S. Lao and X. Qiu, *J. Agric. Food Chem.*, 2018, **66**, 3457–3464.
36 A. P. Richter, B. Bharti, H. B. Armstrong, J. S. Brown, D. Plemmons, V. N. Paunov, S. D. Stoyanov and O. D. Velev, *Langmuir*, 2016, **32**, 6468–6477.
37 L. Dai, R. Liu, L.-Q. Hu, Z.-F. Zou and C.-L. Si, *ACS Sustainable Chem. Eng.*, 2017, **5**, 8241–8249.
38 V. Ugartondo, M. Mitjans and M. P. Vinardell, *Bioresour. Technol.*, 2008, **99**, 6683–6687.
39 B. Hens, Y. Tsume, M. Bermejo, P. Paixao, M. J. Koenigsknecht, J. R. Baker, W. L. Hasler, R. Lionberger, J. Fan, J. Dickens, K. Shedden, B. Wen, J. Wysocki, R. Loebenberg, A. Lee, A. Frances, G. Amidon, A. Yu, G. Benninghoff, N. Salehi, A. Talattof, D. Sun and G. L. Amidon, *Mol. Pharm.*, 2017, **14**, 4281–4294.
40 N. Sun, T. Wang and X. Yan, *RSC Adv.*, 2017, **7**, 9500–9511.
41 Y. Li, X. Qiu, Y. Qian, W. Xiong and D. Yang, *Chem. Eng. J.*, 2017, **327**, 1176–1183.
42 J. Hadgraft and C. Valenta, *Int. J. Pharm.*, 2000, **200**, 243–247.

